Optical properties of well-aligned multiwalled carbon nanotube bundles

M. F. Lin
Department of Physics, National Cheng Kung University, Tainan, Taiwan 701, The Republic of China

F. L. Shyu
Department of Electronics Engineering, Fortune Institute of Technology, Kaohsiung, Taiwan 842, The Republic of China

R. B. Chen
Department of Physics, Yung Ta Institute of Technology & Commerence, Pingtung, Taiwan 909, The Republic of China
(Received 23 September 1999)

The optical properties of well-aligned multiwalled carbon nanotube bundles are studied within the gradient approximation. The imaginary (real) part of the transverse dielectric function exhibits a special peak (dip) at frequency $\omega \sim 2\gamma_0$ (γ_0 is the nearest-neighbor overlap integral). Consequently the loss function shows a prominent π-plasmon peak at $\omega > 2\gamma_0$. The π plasmon also induces a strong and abrupt edge in the reflectance spectrum. These features are similar to those of graphite. The optical properties are hardly affected by the chiral angle of carbon nanotube; moreover, they are insensitive to small variation in the radius of carbon nanotube. On the other hand, the optical properties strongly depend on the polarization direction of an external electric field. The well-aligned multiwalled carbon nanotubes with high radius uniformity, which were recently reported by Fan *et al.* [Science **283**, 512 (1999)], could be used to verify the predicted optical properties.

Carbon nanotubes have attracted a lot of interest since their discovery by Iijima[1] in 1991. A carbon nanotube consists either of a single tubule or of several coaxial tubules with a nanoscaled radius $r \sim 3.4$–150 Å. Carbon atoms are arranged on a cylindrical nanotube in a chiral or a chiral fashion. A single-walled carbon nanotube is a semiconductor or a metal, which depends the radius and the chiral angle.[2–4] When carbon nanotubes are closely packed together, a three-dimensional (3D) carbon nanotube bundle is formed. Carbon nanotube bundles made up of single-walled[5,6] or multiwalled nanotubes[7–9] had been fabricated. The alignment of carbon nanotubes and their size distribution are very important for both fundamental studies and device applications. The single-walled carbon nanotubes in a bundle might bend along the tubular axis.[5,6] To improve the straightness, the well-aligned mutliwalled carbon nanotube bundles were first made by de Heer *et al.*[7] The distribution of the multiwalled nanotube radius ($r \sim 5 \pm 2.5$ nm) was too broad. Only recently, it is possible to largely produce multiwalled carbon nanotube bundles with a narrow radius distribution ($r \sim 8 \pm 1$ nm).[9] These systems enable us to study some essential physical properties of carbon nanotube bundles, say, optical properties. In this work, we study the optical properties of well-aligned multiwalled carbon nanotube bundles, including the transverse dielectric function (ϵ), the loss function, and the reflectance (R). Their dependence on the polarization direction of an external electric field, the chiral angle of carbon nanotube (θ), and the radius of carbon nanotube (r) is investigated. We will also compare these properties between multiwalled carbon nanotube bundles and graphite.[10]

There have been some reports on optical properties of carbon nanotubes, both experimentally and theoretically. The optical ellipsometry was used to directly measure the transverse dielectric function of a multiwalled carbon nanotube bundle.[7] The dielectric function was found to show only a special peak or dip, owing to the superposition of the contributions from the coaxial nanotubes (to be discussed later). Theoretical studies are mainly focused on the optical properties of single-walled carbon nanotube bundles.[11–14] A single-walled carbon nanotube has cylindrical symmetry. Therefore, the magneto-optical absorption spectra exhibit the Aharonov-Bohm quantum oscillation.[11] There are a lot of special structures in the transverse dielectric function,[11–14] since a single-walled carbon nanotube has many 1D subbands. Moreover, the π-electronic collective excitations (π plasmons) lead to a prominent peak in the loss function and a weak edge structure in the reflectance spectrum.[12]

We use the tight-binding model to calculate the π band and the gradient approximation to evaluate the transverse dielectric function. Since carbon nanotubes are highly anisotropic, their optical properties are expected to strongly depend on the polarization direction of an external electric field. In this work, we consider the effects of changes in both the chiral angle of carbon nanotube and the multiwalled nanotube radius. It is important to clarify whether the distribution of multiwalled carbon nanotubes[9] would significantly affect optical properties. Our study shows that there is a special dip (peak) structure in the real (imaginary) part of the transverse dielectric function at $\omega \sim 2\gamma_0$ ($\gamma_0 \simeq 2.4$–3.0 eV is the nearest-neighbor overlap integral[2,4]). The loss function exhibits a pronounced π-plasmon peak at $\omega > 2\gamma_0$. Furthermore, the π plasmon induces a strong and abrupt edge in the reflectance spectrum. The calculated results are consistent with the ellipsometry experiments.[7]

The geometric structure of a single-walled carbon nanotube is uniquely determined by the chiral vector $\mathbf{R}_x = m\mathbf{a}_1 + n\mathbf{a}_2$, which connects two crystallographically equivalent

sites on a 2D graphite sheet.[4] The chiral angle and the radius of a (m, n) nanotube are, respectively, $\theta=\tan^{-1}[-\sqrt{3}n/(2m+n)]$ and

$$r=\frac{|\mathbf{R}_x|}{2\pi}=\frac{b\sqrt{3(m^2+mn+n^2)}}{2\pi} \quad (b=1.42\ \text{Å}).$$

The π band is calculated with the tight-binding model like that employed for a graphite sheet.[15] The energy dispersions and the corresponding wave functions are denoted by $E^{c,v}(k_x,k_y)$ and $\Psi^{c,v}(k_x,k_y)$, respectively.[16] The superscript c (v) represents an unoccupied antibonding π^* band (occupied bonding π band). The transverse wave vector k_x is equal to J/r, where J is the quantized angular momentum adopted as a subband index. The axial wave vector k_y is confined to the first Brillouin zone (BZ). There are two types of electronic structures according to geometric structures. Type-I carbon nanotubes, which correspond to $2m+n\neq 3i$ (i an integer), are semiconductors with energy gap $E_g=\gamma_0 b/r$. Others are metallic type-II carbon nanotubes with $E_g=0$.

We consider a uniform carbon nanotube bundle in which the same multiwalled nanotubes are arranged in a triangular lattice[5] with the intertube distance $d(=3.4\ \text{Å})$.[1] At zero temperature, the inter-π-band excitations from the occupied π-band states to the unoccupied π^*-band states are the only excitation channel. Within the relaxation-time approximation,[17] the transverse dielectric function including all contributions of inter-π-band excitations is given by

$$\epsilon(\omega)=\epsilon_0-\frac{16\pi e^2}{\sqrt{3}(2r+d)^2}\sum_{k_x,k_x',i}\int_{1\text{st BZ}}\frac{dk_y}{2\pi}\times\frac{\left|\left\langle\Psi_i^c(k_x',k_y)\left|\frac{\hat{\mathbf{E}}\cdot\mathbf{P}}{m_e}\right|\Psi_i^v(k_x,k_y)\right\rangle\right|^2}{\omega_{vc,i}^2(k_x,k_x',k_y)}\times\left\{\frac{1}{\omega-\omega_{vc,i}(k_x,k_x',k_y)+i\Gamma}-\frac{1}{\omega+\omega_{vc,i}(k_x,k_x',k_y)+i\Gamma}\right\}, \quad (1)$$

where $\omega_{vc,i}(k_x,k_x',k_y)=E_i^c(k_x',k_y)-E_i^v(k_x,k_y)$ is the inter-π-band excitation energy. The subscript i represents the ith nanotube among the N-shell coaxial nanotubes, ϵ_0 is the background dielectric constant, and Γ is the energy width due to various deexcitation mechanisms. The velocity matrix element $\langle\Psi_i^c(k_x',k_y)|\hat{\mathbf{E}}\cdot\mathbf{P}/m_e|\Psi_i^v(k_x,k_y)\rangle$ is evaluated within the gradient approximation.[17,12] The weak intertube interactions are neglected in Eq. (1). They only affect the low-energy elecronic structure for $E<0.1$ eV.[18,19] The independent nanotube approximation should be a reasonable model for $\omega>0.1$ eV.

The calculations are principally based on the following parameters: $\epsilon_0=2.4$ and $\Gamma=0.033\gamma_0$ (Refs. 12 and 13) [Γ is 0.1 eV for $\gamma_0=3.033$ eV (Ref. 4)]. We construct a multiwalled carbon nanotube[9] with outer radius $r_o=80$ Å and inner radius $r_i=25.5$ Å. The total shell number N is 17. A single-walled nanotube of a fixed radius may have different chiral angles and therefore may have different electronic structures. In this work, we randomly choose nine type-I nanotubes and eight type-II nanotubes. It will be demonstrated that optical properties are not affected by different chiral angles (or the detailed electronic structure of each component nanotube).

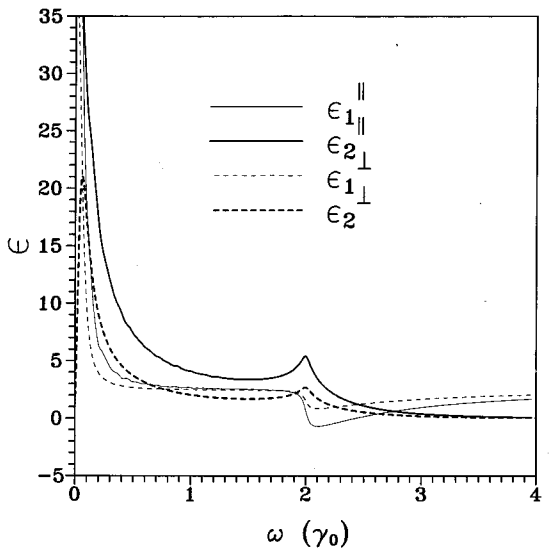

FIG. 1. The real (ϵ_1) and the imaginary (ϵ_2) parts of the transverse dielectric functions are shown for a multiwalled carbon nanotube bundle with shell number $N=17$ at energy width $\Gamma=0.033\gamma_0$. The solid and the dashed curves correspond to the parallel and the perpendicular polarization directions, respectively. The unit of frequency is $2\gamma_0$.

The dielectric functions $\epsilon^{\parallel}$ and $\epsilon^{\perp}$, which, respectively, correspond to the parallel ($\mathbf{E}_{\parallel}\|\hat{\mathbf{y}}$) and the perpendicular ($\mathbf{E}_{\perp}$) polarizations, are evaluated explicitly in this study. We first examine the dielectric function for $\mathbf{E}_{\parallel}$. The selection rule is $\Delta k_y=0$ and $\Delta J=L=0$ [Eq. (1)]. The angular momentum transfer L vanishes. Consequently, only the vertical inter-π-band transitions from the π to the π^* subbands of the same J's are allowed. The dielectric function $\epsilon^{\parallel}$, as shown in Fig. 1 by the solid curves, reveals two main characteristics. Only very weak ripples exist in $\epsilon^{\parallel}$ for $\omega<2\gamma_0$, i.e., $\epsilon^{\parallel}$ is almost featureless in this frequency range. The imaginary (real) part of the dielectric function $\epsilon_2^{\parallel}$ ($\epsilon_1^{\parallel}$) exhibits a prominent peak (dip) structure near $\omega=2\gamma_0$ (at a frequency slightly greater than $2\gamma_0$). These two characteristics could also be found in graphite[10] (to be discussed later).

For the $\mathbf{E}_{\perp}$ case, the selection rule is $\Delta k_y=0$ and $\Delta J=L=\pm 1$. These rules can be easily identified from $\hat{\mathbf{E}}\cdot\mathbf{P}\propto\sin\alpha P_\alpha=(e^{i\alpha}-e^{-i\alpha})P_\alpha/2i$ [in Eq. (1)], where α is the azimuthal angle. Electrons in the occupied π subband of J are excited to the unoccupied π^* subband of $J\pm 1$. The main features in $\epsilon^{\perp}$ (the dashed curves in Fig. 1) are similar to those in $\epsilon^{\parallel}$. Both $\epsilon^{\perp}$ and $\epsilon^{\parallel}$ exhibit no special feature for $\omega<2\gamma_0$ and have similar characteristic structures at $\omega\sim 2\gamma_0$. However, there are two important differences be-

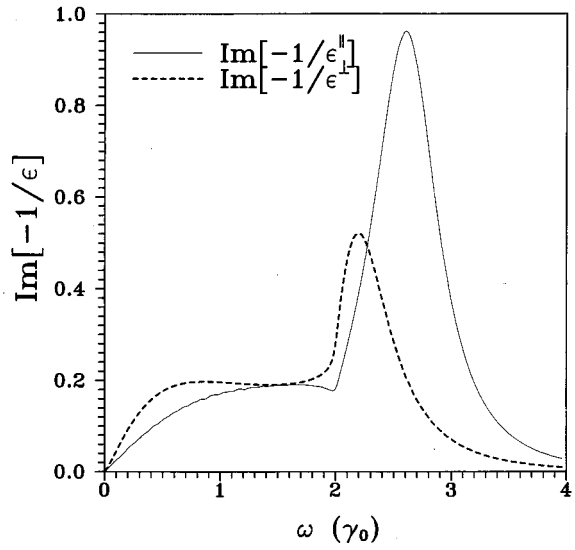

FIG. 2. The loss functions of a multiwalled carbon nanotube bundle are shown for the parallel and perpendicular polarization directions.

tween $\epsilon^{\perp}$ and $\epsilon^{\parallel}$. The minimum excitation energy is $E_i^c(J+1,k_y)-E_i^v(J,k_y)$ for $\mathbf{E}_{\perp}$, so there exists a special peak in $\epsilon_2^{\perp}$ at small $\omega(\sim 0.056\gamma_0)$. The optical transition probability for $\mathbf{E}_{\perp}$ is about half of that for $\mathbf{E}_{\parallel}$. Consequently, $\epsilon_2^{\perp}$ is smaller than $\epsilon_2^{\parallel}$ at all ω's and $\epsilon_1^{\perp}$ is smaller (larger) than $\epsilon_1^{\parallel}$ for $\omega<2\gamma_0$ ($\omega>2\gamma_0$). At $\omega\sim 2\gamma_0$, the special structure in $\epsilon^{\perp}$ is less obvious. This important difference clearly illustrates the strong anisotropy of optical properties. Moreover, it would render the optical spectra for the case of $\mathbf{E}_{\perp}$ relatively weak, e.g., a weaker π-plasmon peak in the loss function (Fig. 2).

The facts that the transverse dielectric function exhibits the special structure at $\omega\sim 2\gamma_0$ and the featureless behavior at $\omega<2\gamma_0$ deserve a closer investigation. Within the tight-binding model,[4,16] the π-electronic states of a single-walled carbon nanotube are derived from those of a graphite sheet. For the hexagonal Brillouin zone of a graphite sheet,[15] the middle point M between the K and K' corners is a saddle point in the energy-wave-vector space. At this k point, the inter-π-band excitation energy is $2\gamma_0$. Each carbon nanotube of the multiple shells must sample some of its eigenstates near the M point. As a result of the flat band structure, such states would lead to a special structure in ϵ at $\omega\sim 2\gamma_0$. We may understand the featureless spectra for $\omega<2\gamma_0$ as follows. Each carbon nanotube has many 1D subbands because of the transverse periodical boundary condition. For example, the number of subbands is more than 70 for a carbon nanotube with $r>20$ Å. Because of to these 1D subbands, a single-walled carbon nanotube bundle[11–14] exhibits many peak structures for $\omega<2\gamma_0$ in addition to the special structure at $\omega\sim 2\gamma_0$. However, for a multiwalled carbon nanotube bundle, the superposition of the coaxial nanotubes would make peaks disappear except the common structure at $\omega\sim 2\gamma_0$. In other words, the mixing effect of the coaxial nanotubes is the cause for the featureless behavior of ϵ at $\omega<2\gamma_0$. In addition, the similarity in the π-electronic structures could explain why multiwalled carbon nanotube bundles and graphite[10] exhibit similar dielectric functions.

Three main features of the transverse dielectric functions are consistent with the ellipsometry experiments.[7] They include a featureless behavior for $\omega<2\gamma_0$, a special peak or dip at $\omega\sim 2\gamma_0$, and a relatively strong peak or dip in the $\mathbf{E}_{\parallel}$ case. Also notice that $\epsilon^{\parallel}$ and $\epsilon^{\perp}$ had been calculated for a single-walled carbon nanotube bundle (Fig. 4 in Ref. 13). A very large energy width ($\Gamma=0.2\gamma_0$) is required to explain the experimental result,[7] the featureless behavior of ϵ at $\omega<2\gamma_0$. The reason for the featureless behavior, as we have pointed out above, should be the superposition of the coaxial carbon nanotubes, instead of a very large Γ.

The transverse dielectric function is used to calculate the loss function $\mathrm{Im}[-1/\epsilon]$ at zero momentum transfer. The dip structure in the real part of the dielectric function leads to a pronounced peak in the loss function, as shown in Fig. 2. This peak is attributed to the collective excitations of π electrons. The π plasmons for $\mathbf{E}_{\parallel}$ (solid curve) and for $\mathbf{E}_{\perp}$ (dashed curve) come from the superposition of $L=0$ and $L=1$ collective excitations of all carbon nanotubes, respectively. The latter has a weaker plasmon peak and a lower plasmon frequency, since the optical excitations are less efficient in the $\mathbf{E}_{\perp}$ case. The π plasmon also exists in graphite.[10] Compared with a multiwalled carbon nanotube bundle, graphite exhibits a stronger plasmon peak and a higher π-plasmon frequency. That graphite has a higher π-electron density could explain the differences for the π plasmon.

The π plasmons at the long-wavelength limit could be measured by the electron-energy-loss spectroscopy (EELS). There are some experimental measurements on a multiwalled carbon nanotube[20–23] as well as a carbon nanotube film.[24,25] The π plasmons are identified from the pronounced peak in the loss spectrum. Using EELS to investigate the π plasmons in a multiwalled carbon nanotube bundle, one needs to specify the direction of the momentum transfer for the probing electrons. For $\mathbf{E}_{\parallel}$ ($\mathbf{E}_{\perp}$), the momentum transfer is parallel (perpendicular) to the nanotube axis. The momentum transfer for both cases is negligible. In addition to the EELS, the optical spectroscopy could also be used to measure the π plasmons. In an experiment, the reflectance spectrum is first measured, then the dielectric function and the loss function are determined by using the Kramers-Kronig relations.[10]

The reflectance is calculated from the relation $R(\omega)=|1-\sqrt{\epsilon(\omega)}|^2/|1+\sqrt{\epsilon(\omega)}|^2$. The spectrum, as shown in Fig. 3, decreases quickly as ω increases from zero. R is essentially featureless for $\omega<2\gamma_0$. When frequency approaches $2\gamma_0$, reflectance begins to increase. R rises to a local maximum at $\omega=2\gamma_0$ and then rapidly drops to a minimum. The abrupt edge in reflectance spectrum is caused by the π plasmon. Also, note that the characteristic peak near the plasmon edge is absent in the spectrum of an ordinary metal.[26] The reflectance spectrum is significantly affected by the polarization directions. Compared to $R^{\perp}$, $R^{\parallel}$ exhibits a relatively pronounced π-plasmon edge structure. The main reason is that the optical response is stronger for the $\mathbf{E}_{\parallel}$ case.

The frequency-dependent characteristics of the reflectance spectrum are similar to those of graphite.[10] The similarities include a rapid decrease and featureless behavior at $\omega<2\gamma_0$, a special peak structure at $\omega=2\gamma_0$, and an abrupt

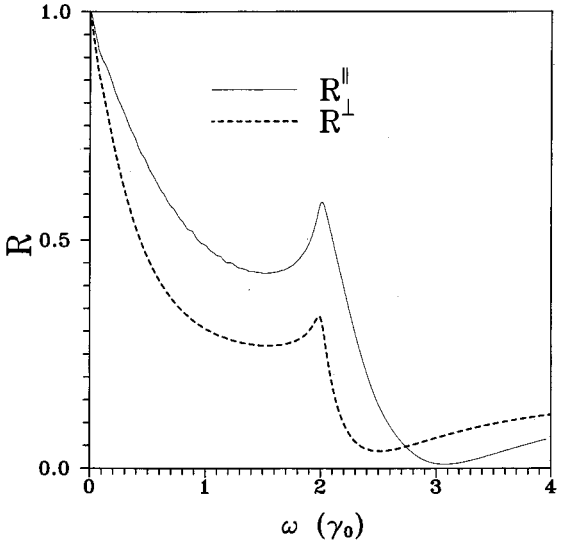

FIG. 3. The reflectance spectra of a multiwalled carbon nanotube bundle are shown for the parallel and perpendicular polarization directions.

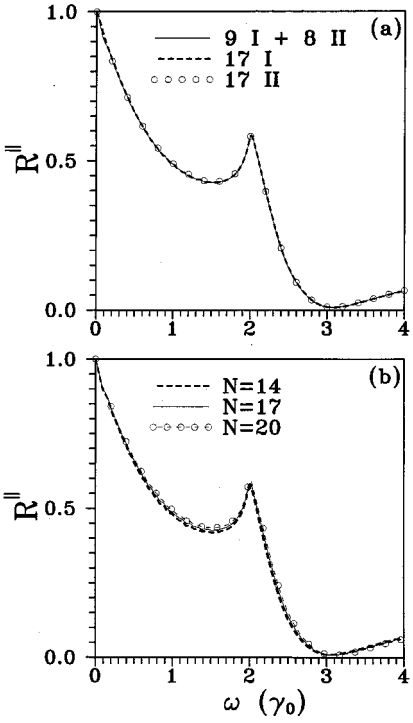

FIG. 4. The reflectance spectra are shown for multiwalled carbon nanotube bundles with (a) different electronic structures and (b) different shell numbers.

π-plasmon edge at $\omega > 2\gamma_0$. In summary, these are three important differences between the multiwalled and the single-walled[12] carbon nanotube bundles in the reflectance spectrum. The reflectance of the latter declines more quickly at $\omega < 2\gamma_0$. It has many oscillational peak structures there. Moreover, its π-plasmon edge structure is weaker. These differences suggest that the reflectance measurements of a multiwalled carbon nanotube bundle are relatively easy.

Figure 4(a) shows the reflectance spectra for multiwalled carbon nanotube bundles with different chiral angles (or electronic structures). A multiwalled carbon nanotube consists of 9 type-I nanotubes and 8 type-II nanotubes, 17 type-I nanotubes, or 17 type-II nanotubes. Apparently the changes in the chiral angles hardly affect the reflectance. This result could be understood from the characteristics of the density of states (DOS). The π-band structures of carbon nanotubes change with the chiral angles, e.g., the number of subbands and the first Brillouin zone. But when the nanotube radius is sufficient large ($r > 25$ Å), DOS at a finite energy width ($\Gamma = 0.03\gamma_0$) is almost independent of the chiral angles except in some small ripple structures. That a single-walled carbon nanotube is only a rolled-up graphite sheet is the main reason. These weak ripples would disappear due to the superposition of the contributions from the coaxial nanotubes. The DOS of a large carbon nanotube is insensitive to the chiral angles, as is the reflectance spectrum. Therefore, the nonuniformity of the multiwalled carbon nanotubes in a 3D bundle is not an important factor in determining the optical properties. On the other hand, the shell number of a multiwalled nanotube (or the multiwalled nanotube radius) would affect the reflectance spectra more effectively. A more compact nanotube bundle exhibits stronger reflectance spectra, mainly owing to more π electrons. The effect of the shell number on R is weak for $\Delta N = 3$ (or $\Delta r = 1$ nm), as shown in Fig. 4(b). This result suggests that a narrow radius distribution $\Delta r \leqslant 1$ nm is required to investigate the main characteristics of the optical properties. Fan *et al.*[9] had successfully made the well-aligned multiwalled carbon nanotube bundle with high radius uniformity ($\Delta r = 1$ nm). This system should be very suitable for measuring the reflectance spectra.

In this work we have studied the optical properties of well-aligned multiwalled carbon nanotube bundles. The transverse dielectric function, the loss function, and the reflectance are calculated within the gradient approximation. The most notable features of the dielectric function are a featureless region for $\omega < 2\gamma_0$, a special peak or dip at $\omega \sim 2\gamma_0$, and a relatively strong peak or dip for the $\mathbf{E}_{\parallel}$ case. Such features are consistent with the ellipsometry measurements.[7] The loss function has a pronounced π-plasmon peak for $\omega > 2\gamma_0$. The π plasmons at the long-wavelength limit could be verified by EELS[20–25] or optical spectroscopy.[10] The reflectance exhibits a rapid decrease and featureless behavior at $\omega < 2\gamma_0$, a special peak structure at $\omega = 2\gamma_0$, and an abrupt π-plasmon edge for $\omega > 2\gamma_0$. The features of the optical properties are similar to those of graphite.[10] The optical properties of well-aligned multiwalled carbon nanotubes are insensitive to small changes in the radius of carbon nanotube. Furthermore, they are independent of the chiral angle of carbon nanotube. However, they are strongly affected by the polarization direction of an external electric field. The well-aligned multiwalled carbon nanotubes with high radius uniformity, which were recently reported by Fan *et al.*,[9] could be used to verify the predicted optical properties.

We thank Y. T. Lu and H. T. Su for a critical reading of the manuscript. This work was supported in part by the National Science Council of Taiwan, and the Republic of China under Grant No. NSC 89-2112-M-006-011.

[1] S. Iijima, Nature (London) **354**, 56 (1991).
[2] J. W. Mintwire, B. I. Dunlap, and C. T. White, Phys. Rev. Lett. **68**, 631 (1992).
[3] N. Hamada, S. I. Sawada, and A. Oshiyama, Phys. Rev. Lett. **68**, 1579 (1992).
[4] R. Saito, M. Fujita, G. Dresselhaus, and M. S. Dresselhaus, Appl. Phys. Lett. **60**, 2204 (1992); Phys. Rev. B **46**, 1804 (1992).
[5] A. Thess *et al.*, Science **273**, 483 (1996).
[6] S. Bandow, S. Asaka, Y. Saito, A. M. Rao, L. Grigorian, E. Richter, and P. C. Eklund, Phys. Rev. Lett. **80**, 3779 (1998).
[7] W. A. de Heer, W. S. Bacsa, A. Chalelain, T. Gerifin, R. Humphrey-Baker, L. Forro, and D. Vargte, Science **268**, 845 (1995).
[8] Z. F. Ren, Z. P. Huang, J. W. Xu, J. H. Wang, P. Buch, M. P. Siegal, and P. N. Provencio, Science **282**, 1105 (1998).
[9] S. Fan, M. G. Chapline, N. R. Franklin, T. W. Tombler, A. M. Cassell, and H. Dai, Science **283**, 512 (1999).
[10] E. A. Taft and H. R. Philipp, Phys. Rev. **138**, A197 (1965).
[11] H. Ajiki and T. Ando, Physica B **201**, 349 (1994).
[12] M. F. Lin and K. W.-K. Shung, Phys. Rev. B **50**, 17 744 (1994).
[13] S. Tasaki, K. Maekawa, and T. Yamabe, Phys. Rev. B **57**, 9301 (1998).
[14] J. W. Mintwire and C. T. White, Synth. Met. **77**, 231 (1996).
[15] P. R. Wallace, Phys. Rev. **71**, 622 (1947).
[16] For the details of the electronic structure see M. F. Lin and D. S. Chuu, Phys. Rev. B **56**, 4996 (1997).
[17] L. G. Johnson and G. Dresselhaus, Phys. Rev. B **7**, 2275 (1973).
[18] R. Saito, G. Dresselhaus, and M. S. Dresselhaus, J. Appl. Phys. **73**, 494 (1993).
[19] Y. K. Kwon and D. Tomanek, Phys. Rev. B **58**, 16 001 (1998).
[20] R. Kuzuo, M. Terauchi, and M. Tanaka, J. Phys. Soc. Jpn. **31**, L1484 (1992).
[21] P. M. Ajayan, S. Iijima, and T. Ichihashi, Phys. Rev. B **47**, 6859 (1993).
[22] V. P. Dravid, X. W. Lin, Y. Wang, X. K. Wang, A. Yee, J. B. Ketterson, and R. P. H. Chang, Science **259**, 1601 (1993).
[23] L. A. Bursill, P. A. Stadelmann, J. L. Peng, and S. Prawer, Phys. Rev. B **49**, 2882 (1994).
[24] R. Kuzuo, M. Terauchi, M. Tanaka, and Y. Saito, Jpn. J. Appl. Phys., Part 2 **33**, L1316 (1994).
[25] T. Pichler, M. Knupfer, M. S. Golden, J. Fink, A. Rinzler, and R. E. Smalley, Phys. Rev. Lett. **80**, 4729 (1998).
[26] J. M. Ziman, *Principles of the Theory of Solids* (Cambridge University Press, Cambridge, 1972).